



Cite this: *RSC Adv.*, 2022, **12**, 11942

## Pyranopyrazole based Schiff base for rapid colorimetric detection of arginine in aqueous and real samples†

Rashim Bawa,<sup>a</sup> Nidhi Deswal,<sup>a</sup> Swati Negi,<sup>a</sup> Manu Dalela,<sup>b</sup> Amit Kumar<sup>c</sup> and Rakesh Kumar  <sup>\*a</sup>

A novel pyranopyrazole-based Schiff base PPS has been synthesized *via* a condensation reaction between aldehyde and hydrazide derivatives of pyranopyrazole. The probe acted as a selective and sensitive chemosensor for the colorimetric detection of arginine under aqueous conditions with a detection limit of  $1.8 \times 10^{-5}$  M. The 1:1 binding stoichiometry was established using various UV-vis spectroscopic methods. A plausible binding mechanism of PPS towards arginine was established *via* <sup>1</sup>H NMR titration techniques and the results were further validated using DFT studies. Moreover, PPS provided a reasonable response for arginine in dietary supplements and human blood plasma which demonstrates its potential application in real sample analysis as well.

Received 6th January 2022  
 Accepted 8th March 2022

DOI: 10.1039/d2ra00091a  
[rsc.li/rsc-advances](http://rsc.li/rsc-advances)

### 1. Introduction

Amino acids form the basic units of biological macromolecular proteins. Referred to as the building blocks of life, amino acids are placed into three different groups based on their requirement in our bodies. The amino acids that are naturally produced by our bodies and are not required in our daily diet are called non-essential amino acids. Essential amino acids are those which cannot be produced by our bodies and are required in our daily diets. However, there are a few amino acids that are essential in certain times of stress or illness as they are required at higher levels than produced by the body. Therefore, these amino acids are called conditionally essential amino acids. Out of the 20 amino acids, arginine is the most alkaline amino acid which is conditionally essential and has the highest isoelectric point (pI = 10.76). It plays a vital role in various biological functions such as the immune system, energizing protein regeneration and promoting the transportation of amino acids.<sup>1</sup> It also promotes wound healing, detoxification of ammonia from the body, cell division and insulin secretion.<sup>2-4</sup> In our bodies, arginine acts as a precursor for the synthesis of several biomolecules. It is an immediate precursor in the biosynthesis of nitric oxide, ornithine, agmatine and urea.<sup>5,6</sup> Due to its

participation in various biological processes; too much or too little presence of arginine or arginine derivatives might lead to different health problems.<sup>7</sup> Therefore, developing viable methods for the detection of arginine has become an emerging area of research.<sup>8-10</sup> Multiple methods for the determination of arginine have currently been reported in the literature, such as electrophoresis, fluorescence spectroscopy, high-performance liquid chromatography and molecular recognition technology.<sup>11-14</sup> However, most of these techniques require complicated laboratory strategies and possess low selectivity which limits their utility. Hence, developing highly selective, fast responsive, inexpensive and simple methods for the recognition of arginine is desirable. Unlike fluorescence chemosensors, which require fluorescence as well as UV-vis apparatus, colorimetric chemosensors are an absolute approach owing to the convenient, sensitive and naked-eye detection ability of analytes based on a visible change in color and a change in absorption spectra.<sup>15-17</sup>

Polyfunctionalized fused heterocyclic compounds such as pyranopyrazoles and their derivatives have been highly emphasized in organic chemistry because of their structural resemblance to biologically active coumarin. The benzene ring of coumarin is substituted by a bioactive pyrazole ring to form pyranopyrazole, which is widely used as a parent compound to synthesize different natural products with biological significance.<sup>18</sup> Like coumarins, pyranopyrazoles are also found to have anticancer,<sup>19</sup> antimicrobial,<sup>20</sup> anti-inflammatory<sup>21</sup> and analgesic<sup>22</sup> properties. A number of coumarin derivatives have been synthesized and used for the selective recognition of ions<sup>23,24</sup> and neutral species.<sup>25,26</sup> However, although a variety of pyranopyrazole derivatives have been synthesized, their utility as chemosensors has rarely been explored. To the best of our

<sup>a</sup>Bioorganic Laboratory, Department of Chemistry, University of Delhi, Delhi, 110007, India. E-mail: rakeshkp@gmail.com

<sup>b</sup>Stem Cell Facility (Centre of Excellence for Stem Cell Research), All India Institute of Medical Sciences, New Delhi, 110029, India

<sup>c</sup>Department of Chemistry, Dyal Singh College, University of Delhi, Delhi, 110003, India

† Electronic supplementary information (ESI) available. See DOI: [10.1039/d2ra00091a](https://doi.org/10.1039/d2ra00091a)



knowledge, we were the first group to develop a pyranopyrazole-based colorimetric sensor for the recognition of  $\text{Fe}^{3+}$  ions.<sup>27</sup> In the present work, we have aimed at developing a novel Schiff base linked pyranopyrazole derivative (**PPS**) through a convenient synthetic route in good yield that acts as a potential colorimetric chemosensor for arginine.

## 2. Experimental

### 2.1 Materials and methods

The reagents and the solvents used for the synthesis and UV-vis studies were of analytical and spectroscopic grade. Phenyl hydrazine, hydrazine hydrate, ethyl 2-chloroacetate and ethyl acetoacetate were purchased from Spectrochem Pvt. Ltd and were used without further purification. All the amino acids used in UV-vis studies were purchased from Sigma Aldrich and Spectrochem Pvt Ltd.  $^1\text{H}$  and  $^{13}\text{C}$  NMR were recorded at room temperature on a JNM-EXCP 400 (JEOL, USA) spectrometer using TMS as an internal standard and the chemical shifts are reported in parts per million (ppm). FTIR data was recorded using a Shimadzu IR Affinity 1S Spectrophotometer. The crude products were purified using column chromatography (silica gel 100–200 mesh) and methanol–chloroform as the solvent system. UV-vis experiments were performed on a Carey Series UV-vis spectrophotometer using a 1 cm quartz cuvette. All experiments were performed in compliance with the policy statement on ethical considerations involved in research on human subjects (ICMR, 1980). These experiments were approved by the departmental research committee of University of Delhi. The blood sample of a healthy volunteer was procured from a local pathology lab and arginine granule supplements were commercially available in the market. The donor provided informed consent in accordance with the guidelines of the institution.

### 2.2 Synthesis of ethyl 2-(3,4-dimethyl-6-oxopyrano[2,3-*c*]pyrazol-2(6*H*)-yl) acetate (2)

Anhydrous  $\text{K}_2\text{CO}_3$  (2 mmol) was added to a solution of 3,4-dimethylpyrano[2,3-*c*]pyrazol-6(2*H*)-one (**1a**) (5 g, 1 mmol) in acetonitrile. To this ethyl 2-chloroacetate (2 mmol) was added drop-wise with constant stirring (Scheme 1). The reaction mixture was refluxed and the progress of the reaction was monitored through TLC. After completion of the reaction (6 h), the reaction mixture was allowed to cool to room temperature and then filtered to remove the solid precipitate. The filtrate obtained was concentrated under reduced pressure. The resultant crude product was recrystallized from ethanol as a white solid in 75% yield. The melting point was found to be 145–147 °C.

$^1\text{H}$  NMR (400 MHz, DMSO- $d_6$ ):  $\delta$  5.88 (s, 1H), 5.12 (s, 2H), 4.17 (q,  $J = 7.1$  Hz, 2H), 2.48 (s, 3H), 2.40 (s, 3H), 1.22 (t,  $J = 7.1$  Hz, 3H).  $^{13}\text{C}$  NMR (100 MHz, DMSO- $d_6$ ):  $\delta$  168.0, 161.1, 158.2, 152.6, 138.8, 108.2, 102.0, 61.9, 50.9, 19.2, 14.5, 11.4. HRMS ( $m/z$ ): calculated for  $\text{C}_{12}\text{H}_{14}\text{N}_2\text{O}_4$  [M + H]<sup>+</sup> 251.0987; found 251.0980.

### 2.3 Synthesis of 2-(3,4-dimethyl-6-oxopyrano[2,3-*c*]pyrazol-2(6*H*)-yl) acetohydrazide (3)

To a solution of 2 (3 g, 1 mmol) in ethanol, hydrazine hydrate (2 mmol) was added and the mixture was heated under reflux conditions (Scheme 1). The reactant was consumed completely within 4 h, as monitored by TLC. After cooling in ice conditions, the resultant precipitates were filtered and washed with cold ethanol to obtain 3 as a white solid in 87% yield and melting point range was 282–284 °C.

$^1\text{H}$  NMR (400 MHz, DMSO- $d_6$ ):  $\delta$  9.34 (s, 1H), 5.82 (s, 1H), 4.72 (s, 2H), 4.30 (s, 2H), 2.45 (s, 3H), 2.35 (d,  $J = 1.2$  Hz, 3H).  $^{13}\text{C}$  NMR (100 MHz, DMSO- $d_6$ ):  $\delta$  165.8, 161.2, 158.1, 152.7, 107.8, 101.9, 50.8, 19.2, 11.7. HRMS ( $m/z$ ): calculated for  $\text{C}_{10}\text{H}_{12}\text{N}_4\text{O}_3$  [M + H]<sup>+</sup> 237.0943; found 237.0984.

### 2.4 Synthesis of 2-(3,4-dimethyl-6-oxopyrano[2,3-*c*]pyrazol-2(6*H*)-yl)- $N'$ -(3-methyl-6-oxo-1-phenyl-1,6-dihydropyrano[2,3-*c*]pyrazol-4-yl)methylene) acetohydrazide (PPS)

As shown in Scheme 2, 3 (200 mg, 2 mmol) and 4 (1 mmol) were mixed in ethanol by subsequently adding few drops of glacial acetic acid. The reaction mixture was then refluxed and product formation was observed through TLC. The reaction was complete in 6 h and the reaction mixture was allowed to cool under ice conditions. The precipitates then obtained were filtered and washed with cold ethanol to obtain a pale green solid as the crude product. The product was then purified using column chromatography (CHCl<sub>3</sub>–MeOH, 9 : 1) to procure **PPS** as a pale yellow solid in 70% yield. The melting point of **PPS** was found to be 292–294 °C.

$^1\text{H}$  NMR (400 MHz, DMSO- $d_6$ ):  $\delta$  12.29 (s, 1H), 8.27 (s, 1H), 7.77–7.42 (m, 5H), 6.43 (s, 1H), 5.86 (s, 1H), 5.48 (s, 1H), 5.07 (s, 1H), 2.54 (s, 3H), 2.48 (s, 3H), 2.40 (s, 3H).  $^{13}\text{C}$  NMR (100 MHz, DMSO- $d_6$ ):  $\delta$  168.7, 161.1, 159.3, 158.0, 152.5, 151.2, 145.6, 144.3, 139.1, 138.4, 136.8, 130.0, 127.9, 121.5, 121.2, 107.9, 102.0, 99.8, 51.0, 19.1, 17.4, 15.9, 11.5. HRMS ( $m/z$ ): calculated for  $\text{C}_{24}\text{H}_{20}\text{N}_6\text{O}_5$  [M + H]<sup>+</sup> 473.1529; found 473.1579.

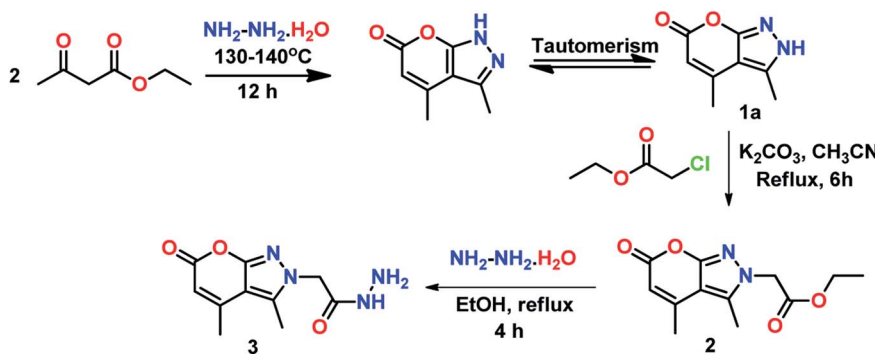
### 2.5 UV-vis studies

To explore the interactions of **PPS** with various amino acids, UV-vis experiments were performed. A stock solution of **PPS** (10 mM) was prepared in DMSO and stock solutions of 100 mM of the amino acids alanine, valine, cystine, glycine, glutathione, homocystine, histidine, leucine, lysine, phenylalanine, proline and serine were prepared in double-distilled water. The stock solutions of amino acids were stored at 4 °C and used within ten days of preparation. To carry out the binding studies, 10  $\mu\text{M}$  of **PPS** solution was prepared in DMSO–PBS (8 : 2 v/v, 10 mM, pH = 7.4). 30  $\mu\text{L}$  of stock solution of an amino acid was added to 2.97 mL of **PPS** (10  $\mu\text{M}$ ) in a quartz cuvette. The absorption spectra of **PPS** were recorded in the absence and presence of various amino acids.

### 2.6 Selectivity studies

To analyze the interference by other amino acids in the recognition of arginine, competitive binding studies were performed. To achieve this, the colorimetric and spectral changes of **PPS**





Scheme 1 Synthetic route to compounds 2 &amp; 3.

arginine (10 : 5  $\mu\text{M}$ ) were observed in the presence of 5  $\mu\text{M}$  of other amino acids.<sup>28</sup>

## 2.7 Binding stoichiometry analysis & limit of detection

The binding affinity of **PPS** with arginine was examined through absorption titration experiments by successive additions of arginine (0–20  $\mu\text{M}$  with an interval of 2  $\mu\text{M}$ ). The absorption spectra thus obtained were used to construct a Benesi–Hildebrand plot of  $1/(A - A_0)$  vs.  $1/[\text{Arg}]$ . The binding constant was calculated from the slope of the B–H plot from eqn (1):

$$\frac{1}{(A - A_0)} = \frac{1}{K_b(A_{\max} - A_0)C} + \frac{1}{(A_{\max} - A_0)} \quad (1)$$

Here  $A_0$  and  $A$  are the absorption intensities of **PPS** in the absence and presence of arginine, respectively.  $C$  is the concentration of arginine,  $K_b$  is the binding constant and  $A_{\max}$  is the maximum absorption intensity observed after the addition of arginine.

To find the binding stoichiometry, stock solutions of **PPS** (10  $\mu\text{M}$ ) and arginine (10  $\mu\text{M}$ ) were prepared in DMSO-PBS (8 : 2 v/v, 10 mM, pH = 7.4) and double-distilled water, respectively. Then 0.3–3 mL of **PPS** and 3–0.3 mL of arginine were added respectively to keep the total volume in the quartz cuvette at 3 mL for recording the absorption spectra. The Job's plot was obtained by plotting a graph between mole fraction of **PPS** ( $X_{\text{PPS}}$ ) and  $(A_0 - A) \times X_{\text{PPS}}$ .<sup>29</sup>

The limit of detection of **PPS** for arginine was calculated using eqn (2):

$$\text{LOD} = \frac{3\sigma}{S} \quad (2)$$

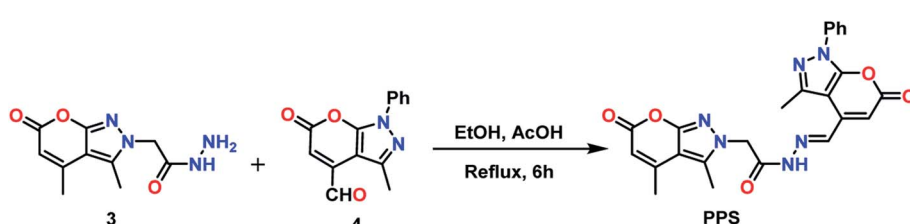
Ten replicate absorption measurements were taken to calculate standard deviation ( $\sigma$ ) and  $S$  is the slope of the calibration curve.

## 2.8 Computational methods

The binding interactions of the synthesized ligand with amino acid arginine were studied theoretically based on the Density Functional Theory (DFT) method using the Gaussian 09 program at the B3LYP/6-311++G(d,p) level of theory.<sup>30</sup> A TD-DFT study was carried out by employing a hybrid B3LYP and 6-311+G basis set in Gaussian 09. Careful analysis of the vibrational frequencies confirms that all the stationary points in the way of geometrical optimization correspond to local minima. The sum of electronic energy ( $\epsilon_0$ ) and thermal free energy ( $G_{\text{corr}}$ ) were used in the computation of  $\Delta G$  values. The integral equation formalism polarized continuum model (IEFPCM) was employed for single point time-dependent DFT (TD-DFT) calculations on the optimized geometry in order to account for the solvent effect of DMSO.<sup>31</sup>

## 2.9 Hemolysis assay

The blood compatibility of **PPS** was studied using a hemolysis assay. Briefly, blood was collected from a healthy voluntary human donor in a heparinized tube, centrifuged for 5 min at 4 °C, and the pellet (cells) washed 3 times with 1 × PBS (pH = 7.4) as described previously.<sup>32</sup> The human RBCs were treated with different concentrations of **PPS** (10, 25, 50, and 100  $\mu\text{M}$ ) for 1 h at 37 °C. The amount of hemoglobin released was analyzed with a microplate reader at 540 nm and the percentage of hemolysis was calculated using eqn (3):



Scheme 2 Synthetic route to PPS.





Fig. 1 Colorimetric variations in PPS ( $10 \mu\text{M}$ ) on addition of 10 equiv. of different amino acids.

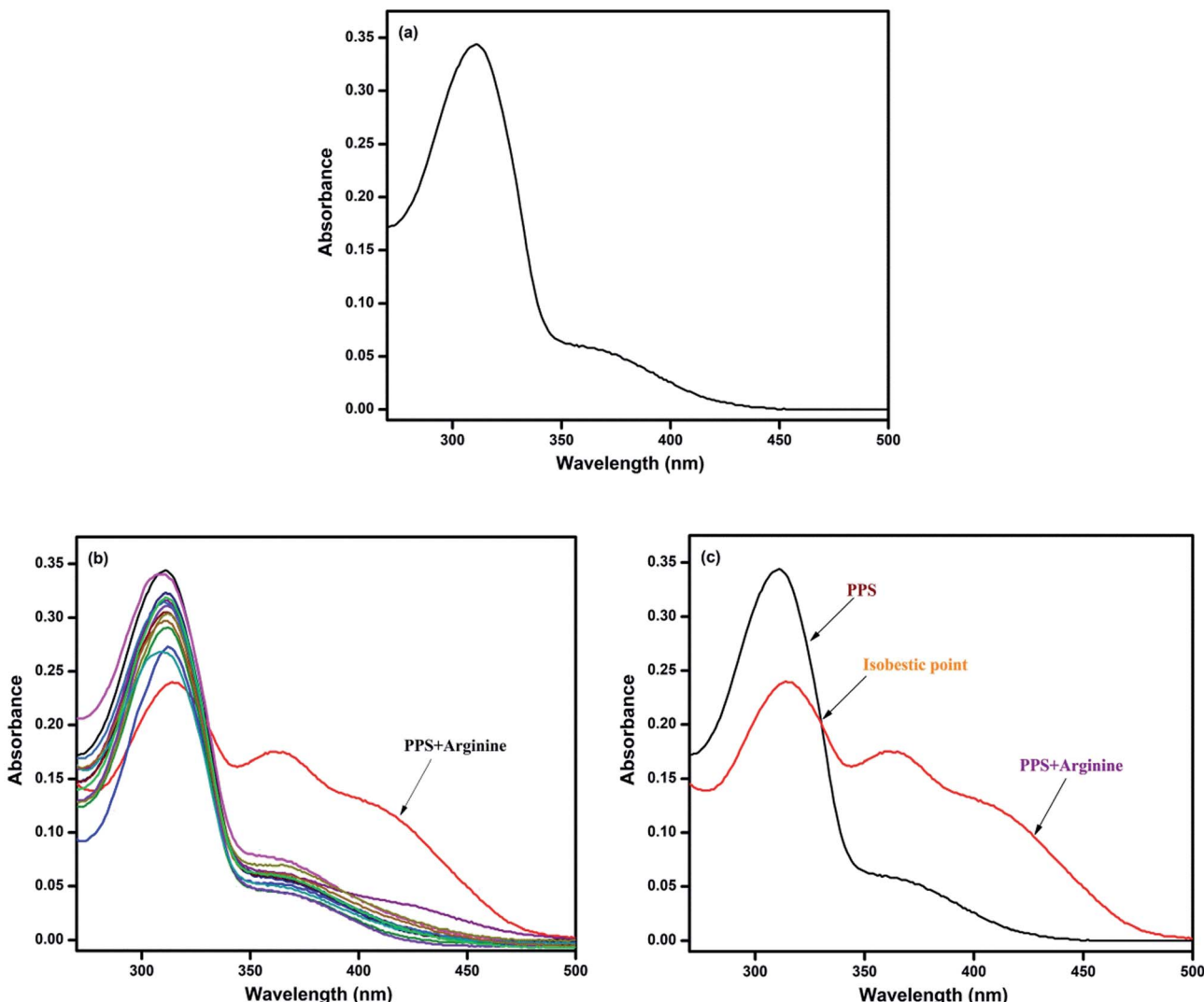


Fig. 2 (a) Absorption spectrum of PPS ( $10 \mu\text{M}$ ) in DMSO-PBS (8 : 2 v/v,  $10 \text{ mM}$ ,  $\text{pH} = 7.4$ ). (b) Spectral changes in PPS on addition of 10 equiv. of different amino acids. (c) Absorption spectra of PPS and PPS + arginine.



$$\text{Hemolysis (\%)} = \frac{\text{Sample}_{540\text{nm}} - \text{Negative control}_{540\text{nm}}}{\text{Positive control}_{540\text{nm}} - \text{Negative control}_{540\text{nm}}} \times 100 \quad (3)$$

1% Triton X-100 was used as a positive control which achieved complete hemolysis (100%) and 1× PBS (pH = 7.4) served as the negative control. All the experiments were performed in triplicate. After incubation, the RBCs were again isolated by centrifugation, resuspended in 1× PBS, mounted on a wet slide and examined using a bright field light microscope.

### 3. Results and discussions

#### 3.1 Synthesis

The final product **PPS** was synthesized by mixing ethanolic solutions of **3** and **4** and adding a few drops of acetic acid to

the resulting reaction mixture. This reaction mixture was refluxed for 6 h to obtain **PPS** in 70% yield. The precursors of the final compound **PPS** were synthesized from their parent molecules **1a** and **1b** which were prepared using a modified Pechmann condensation reaction of ethyl acetoacetate with hydrazines at 130–140 °C through *in situ* generation of pyrazolone (Scheme S1†). Reactant **4** was synthesized by oxidation of 3,4-dimethyl-1-phenylpyrano[2,3-*c*]pyrazol-6(1*H*)-one (**1b**) in the presence of selenium dioxide and 1,4-dioxane as solvent, under reflux conditions, as already reported by our research group (Scheme S2†).<sup>33</sup> The formation of all the synthesized compounds was confirmed by <sup>1</sup>H NMR, <sup>13</sup>C NMR, FT-IR and mass spectroscopy.

#### 3.2 Colorimetric recognition of arginine

The colorimetric sensing of ligand **PPS** was investigated by the addition of thirteen different amino acids to solutions of **PPS**. Only in the case of the addition of arginine was an immediate

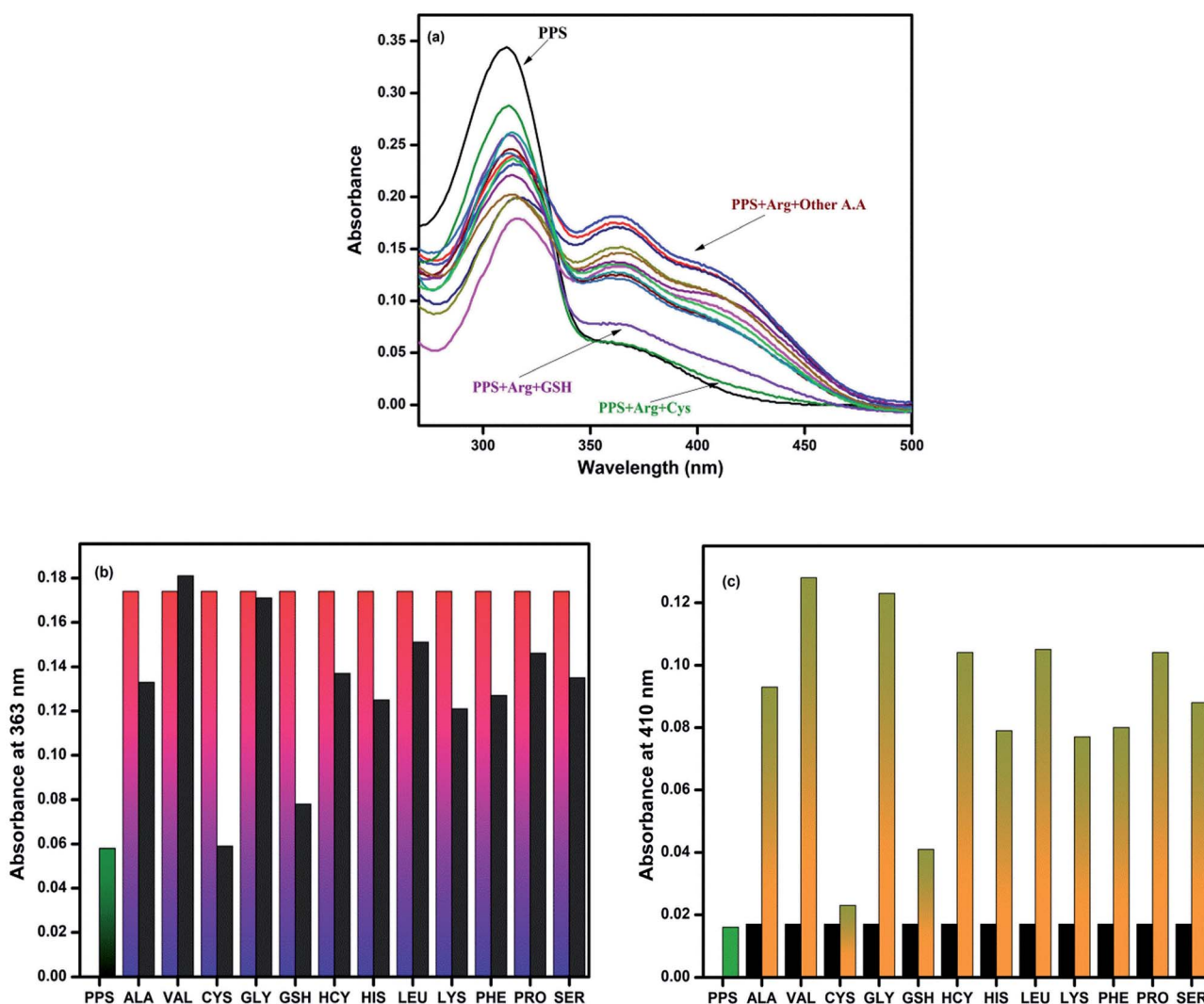


Fig. 3 (a) Absorption spectral changes of PPS in DMSO-PBS (8 : 2 v/v, 10 mM, pH = 7.4) on addition of different amino acids in the presence of arginine. (b) Absorbance data for PPS and amino acids at 363 nm. (c) Absorbance data for PPS and amino acids at 410 nm.



remarkable change from colorless to yellow observed while no color changes were observed on the addition of the other amino acids (Fig. 1).

### 3.3 Absorption studies

The UV-vis absorption spectrum of **PPS** (10  $\mu$ M) recorded in DMSO-PBS (8 : 2 v/v, 10 mM, pH = 7.4) displayed a broad band in the range of 270–500 nm with an absorption maximum at 310 nm (Fig. 2a) which might be attributed to the  $\pi$ - $\pi^*$  or n- $\pi^*$  transitions within the ligand. When 10 equiv. of amino acids, such as alanine, valine, cystine, glycine, glutathione, homocystine, histidine, leucine, lysine, phenylalanine, proline and serine, were added to the stock solution of **PPS**, no significant changes were observed in its absorption spectra. However, the addition of arginine to **PPS** resulted in a prominent change in the absorption spectra, as shown in Fig. 2(b). It can be seen in Fig. 2(c) that in the presence of arginine, the intensity of the charge transfer band of **PPS** centered at 310 nm

prominently decreased with a red shift of 5 nm while the absorption intensity at 363 nm increased. Furthermore, a new band appeared at 410 nm with an isobestic point at 330 nm, suggesting the formation of a stable complex between **PPS** and arginine.

### 3.4 Selectivity studies

To assess the selectivity of **PPS** for arginine in the presence of a complex background of other co-existing competitive amino acids, an interference experiment was carried out, as shown in Fig. 3. The experiment revealed in Fig. 3(a) that the absorption spectra of **PPS** containing arginine (5 equiv.) showed similar patterns in the presence of other amino acids (5 equiv.). However, slight interference was observed with CYS and GSH. Based on the response towards the interfering samples, the chemosensor **PPS** showed selectivity for arginine in the presence of other amino acids except CYS and GSH under the same conditions (Fig. 3(b) and (c)).

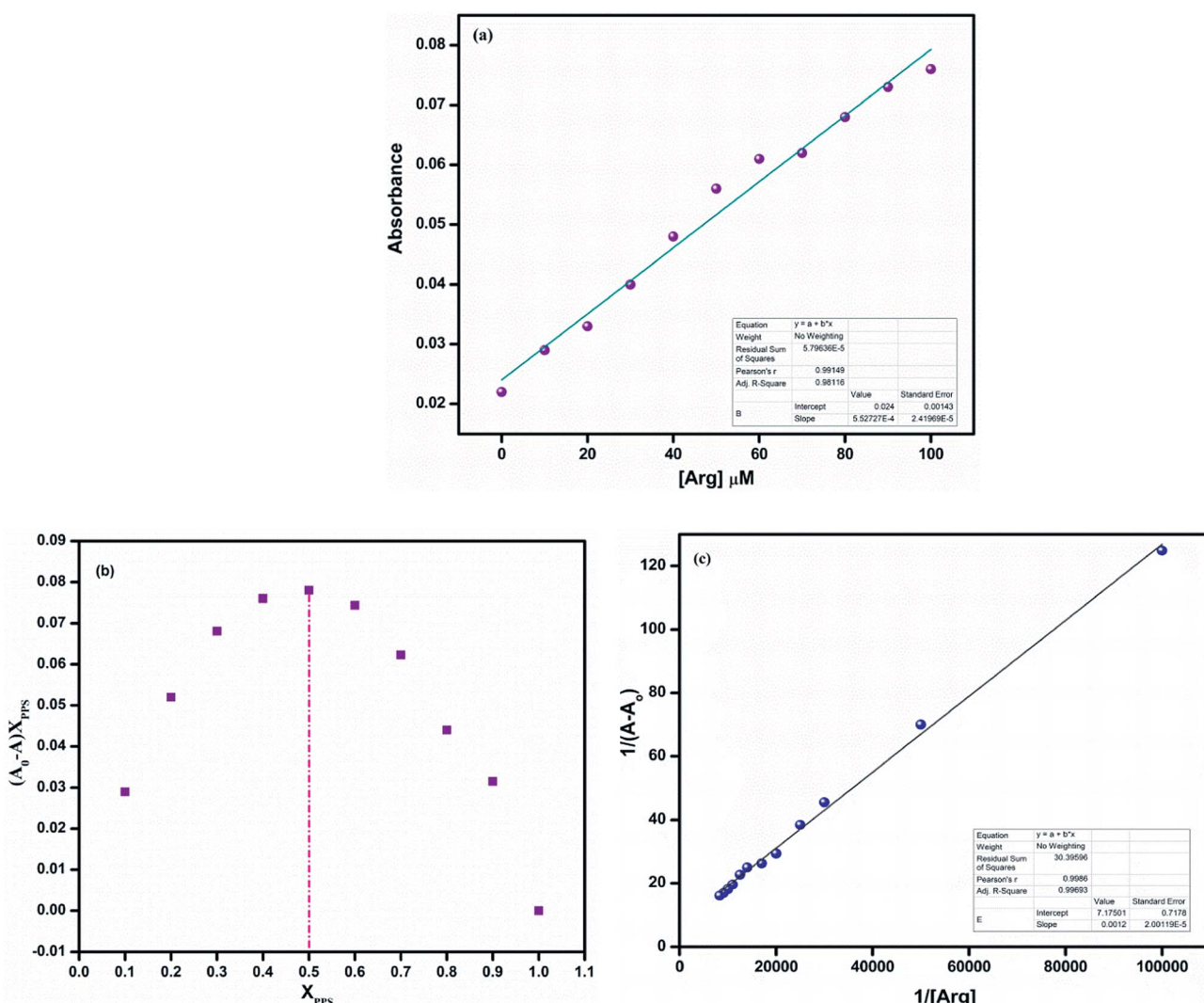


Fig. 4 (a) Absorption intensity of **PPS** (10  $\mu$ M) on subsequent addition of arginine (0–100  $\mu$ M). (b) Job's plot of **PPS** with arginine in DMSO-PBS (8 : 2 v/v, 10 mM, pH = 7.4). (c) B-H plot of **PPS** with arginine in DMSO-PBS (8 : 2 v/v, 10 mM, pH = 7.4).



### 3.5 Binding stoichiometry analysis

To get further perceptions on the interaction between the ligand **PPS** and arginine, titration experiments were carried out in DMSO–PBS (8 : 2 v/v, 10 mM, pH = 7.4). On successive addition of arginine to **PPS**, it could be observed that the absorption intensity at 410 nm gradually increased (Fig. 4(a)).

Furthermore, to recognize the coordination of **PPS** with arginine, the binding constant and the binding stoichiometry were determined using a Job's plot and Benesi–Hildebrand plot, respectively. In the Job's plot (Fig. 4(b)), it could be observed that the maximum was achieved when the molar ratio of the chemosensor was 0.5. This suggested 1 : 1 binding stoichiometry between **PPS** and arginine. The B–H plot of  $1/(A - A_0)$  vs.  $1/[\text{Arg}]$  showed linearity with  $R^2 = 0.99693$ , which also confirmed the 1 : 1 binding stoichiometry of the complex (Fig. 4(c)). The binding/association constant of **PPS** for arginine was found to be  $1.57 \times 10^4 \text{ M}^{-1}$ .

### 3.6 Limit of detection & time response

The limit of detection was calculated to be  $1.8 \times 10^{-5} \text{ M}$ . This implied that the ligand **PPS** could be used for quantitative detection of arginine even at low concentrations. The absorbance of **PPS** (10  $\mu\text{M}$ ) at 410 nm changed immediately when 1 equiv. of arginine was added and remained constant afterwards (Fig. 5). The ultrafast sensing of **PPS** made it suitable for the real-time detection of arginine.

### 3.7 Plausible sensing mechanism

The binding modes of **PPS** with arginine were further studied through  $^1\text{H}$  NMR titration experiments. Upon addition of 0.5

equiv. of arginine to **PPS** in  $\text{DMSO}-d_6$ , the peak at 12.29 ppm was almost completely suppressed. However, no other changes were observed in the NMR spectrum (Fig. S7†). This suggested that the binding of arginine to **PPS** occurred through the –NH proton of the Schiff base unit present in **PPS**. The plausible binding mechanism is shown in Scheme S3.† The mechanism draws further support from the observations from computational studies in the following section.

### 3.8 Computational studies

DFT calculations were performed with the objective of gaining an insight into the binding interaction of **PPS** with arginine. A strong binding interaction is indicated in the **PPS**–arginine complex exhibiting free energy,  $\Delta G = -13.6 \text{ kcal mol}^{-1}$  for the formation of the complex *via* H-bonding. As per the energetic considerations, it is interesting to note that the ligand undergoes a conformational change, from **PPS (a)** to **PPS (b)** in the structure of the molecule, thereby allowing for efficient binding to arginine at two different sites in order to form a more stable complex structure (Fig. S8†). It is evident from Fig. 6 that hydrogen bonds of the type N–H–N have been formed at two different binding sites that are represented as  $\text{N}_{59}\text{--H}_{29}\text{--N}_{13}$  (site 1) and  $\text{N}_{44}\text{--H}_{68}\text{--N}_{56}$  (site 2) with H-bond distances of 1.87 Å and 2.17 Å, respectively. Natural bond orbital (NBO) analysis was also performed to investigate the relative strength of these binding interactions in the **PPS**–arginine complex. The stabilization energies for intermolecular interactions, between the lone-pair electrons of the proton acceptor and antibonding orbitals of the proton donor, obtained using second-order perturbation theory as implemented in the NBO analysis,

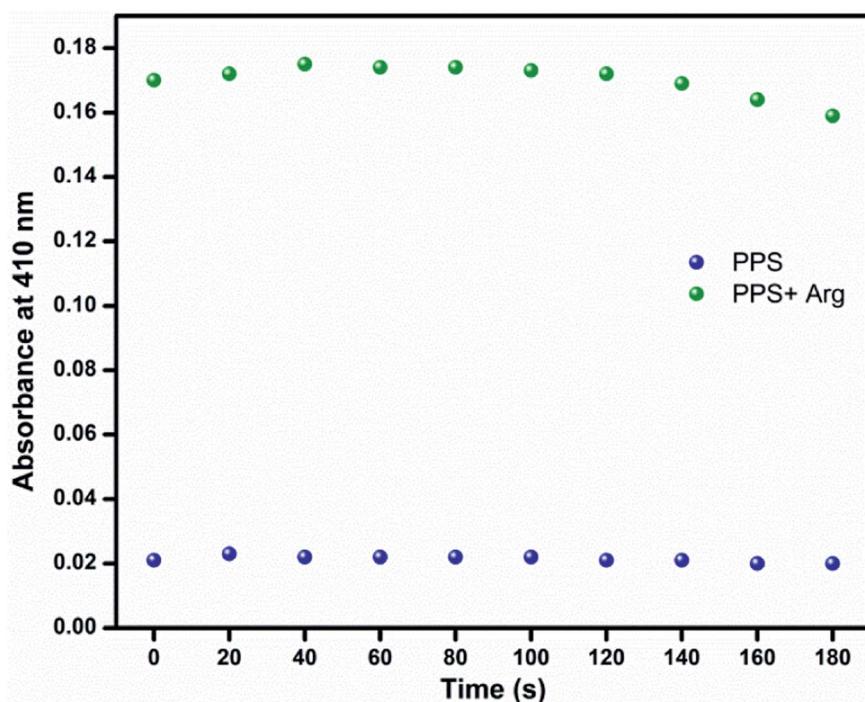


Fig. 5 Time-dependent absorption response of PPS (10  $\mu\text{M}$ , DMSO–PBS, pH = 7.4, 8 : 2, v/v) at 410 nm in the presence of 1 equiv. of arginine.



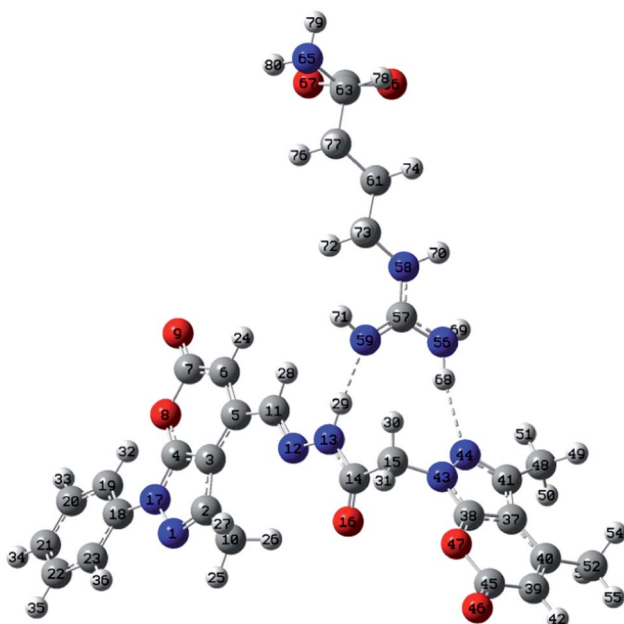


Fig. 6 Most stable configuration of PPS-arginine complex.

account for stronger interaction at site 1 ( $7.36 \text{ kcal mol}^{-1}$ ) compared to site 2 ( $3.77 \text{ kcal mol}^{-1}$ ). These trends in stabilization energies are in accord with the observed H-bond distances at the two different sites in the complex.

The TD-DFT computations were aimed at achieving better insight into and a thorough understanding of the nature of the transitions in the UV-vis spectra. A careful analysis of the electronic states of PPS and PPS-arginine suggested that a set of

closely populated occupied MOs (Fig. S9 & S10<sup>†</sup>) are involved in electronic excitation (at  $\lambda_{\max}$ ) which are primarily represented by electronic transitions from HOMO-5 to LUMO. The electron density in the PPS-arginine complex in HOMO-5 is primarily centered on arginine, which indicates a charge transfer from arginine to PPS in the complex. The HOMO and LUMO orbitals corresponding to PPS and the PPS-arginine complex have been depicted in Fig. 7. The calculated energy gap ( $\Delta E$ ) between HOMO and LUMO was found to be lower than that of the free ligand, illustrating the occurrence of a red shift on the addition of arginine to PPS.

The results of the TD-DFT study clearly revealed a red shift in the absorption maximum of the ligand from 303 nm to 319 nm, upon complexation with arginine. Moreover, the oscillator strength of the specified primary transition was also observed to decrease from 0.9423 to 0.1814, which accounts for the decrease in absorption intensity at  $\lambda_{\max}$  in the UV-vis spectra of the ligand upon complexation. These results thus exhibit reasonable agreement with the experimentally observed UV-vis spectra. It may be noted that the TD-DFT computations tend to overestimate or underestimate energies of the excited states<sup>34,35</sup> owing to the local nature and asymptotic behavior of the approximate functional with special reference to the exchange correlation functional in the case of charge transfer transitions. Consequently, we observe deviations of  $\lambda_{\max}$  values in theoretically obtained UV-vis spectra in comparison to the experimental spectra (Table S2<sup>†</sup>).

### 3.9 Reversibility

The most important aspect for a sensor to be employed for practical applications is its reversibility and recyclability. We

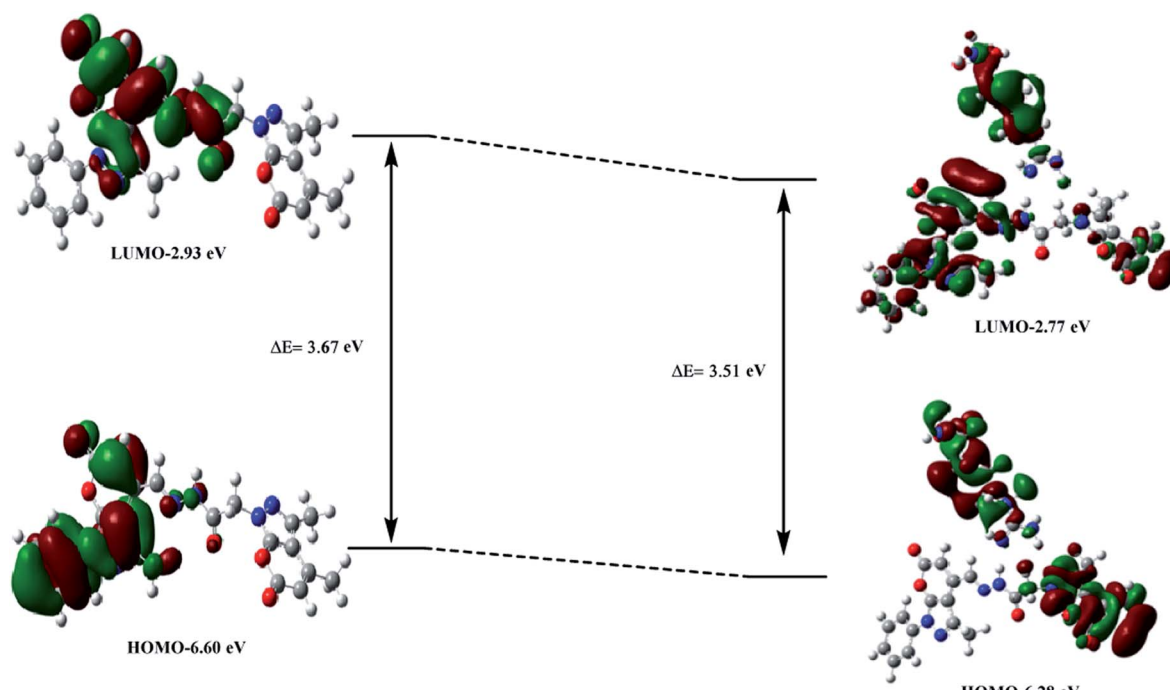


Fig. 7 The HOMO-LUMO gap calculated by DFT studies.



have seen that **PPS** has proved to be sensitive towards arginine. However, there have been literature reports<sup>36</sup> that arginine has the ability to bind phosphates through electrostatic interactions. Therefore, to examine the reversibility of **PPS**-arginine, we selected  $\text{H}_2\text{PO}_4^-$  ions. It was observed that on successive additions of  $\text{H}_2\text{PO}_4^-$ , the absorption intensity of the band due to **PPS**-arginine (at 410 nm) decreased while that due to **PPS** alone (310 nm) started to increase (Fig. 8(a)). The absorption intensity at 410 nm has also been plotted against increasing concentration of  $\text{H}_2\text{PO}_4^-$  (Fig. 8(b)). Moreover, a naked-eye color change from yellow to colorless was also noticed, which further supported the reversibility. Hence, **PPS** exhibited good reversibility and has the potential to be used in practical applications.

### 3.10 Hemolysis study

The *in vitro* blood biocompatibility and hemolysis of **PPS** was studied at various concentrations (10, 25, 50, and 100  $\mu\text{M}$ ). After incubation, human RBCs remain unaffected by all concentrations of **PPS** while complete membrane damage to RBCs (hemolysis) was observed in 1% Triton X-100 (positive control), as shown in Fig. 9. No hemolysis was observed in saline (negative control) whereas **PPS** showed 3–8% hemolysis after incubation for 1 h at 37 °C which was not significant, indicating its blood compatibility nature.

### 3.11 Real sample analysis

**3.11.1 Detection of arginine in arginine supplements.** To examine the practical utilization of the chemosensor **PPS**

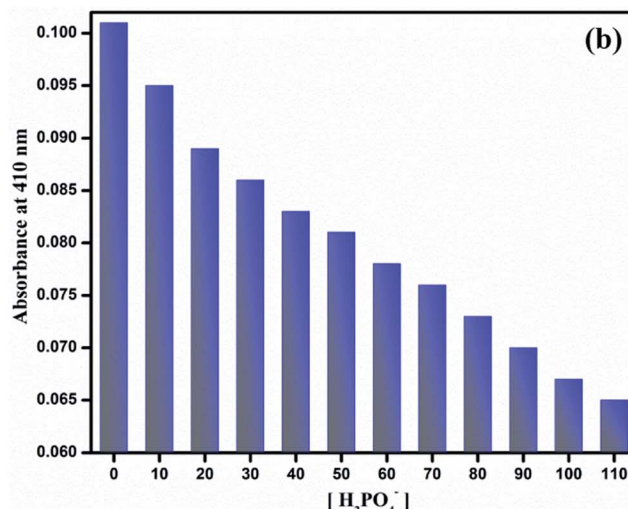
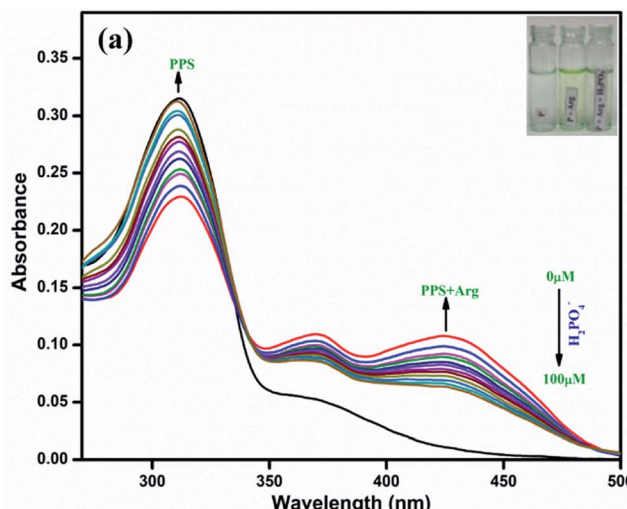


Fig. 8 (a) Absorption spectra of **PPS** (10  $\mu\text{M}$ , DMSO–PBS, pH = 7.4, 8 : 2, v/v) with arginine (100  $\mu\text{M}$ ) and successive additions of  $\text{KH}_2\text{PO}_4$  (0–100  $\mu\text{M}$ ). (b) Absorbance of **PPS**–arginine (10 : 100  $\mu\text{M}$ , DMSO–PBS, pH = 7.4, 8 : 2, v/v) at 410 nm vs. increasing concentration of  $\text{H}_2\text{PO}_4^-$ .

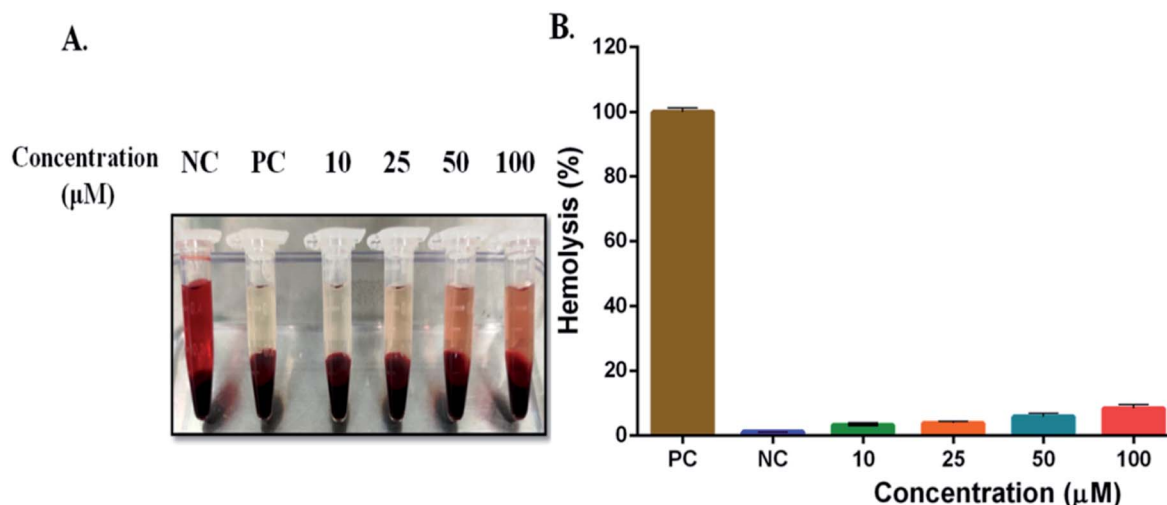


Fig. 9 Hemolysis assay. (A) RBCs were incubated with **PPS** at different concentrations for 1 h at 37 °C. Triton X-100 (1%) and normal saline were used as positive and negative controls (PC & NC), respectively. (B) Quantitative estimation of RBCs membrane damage and haemoglobin release.



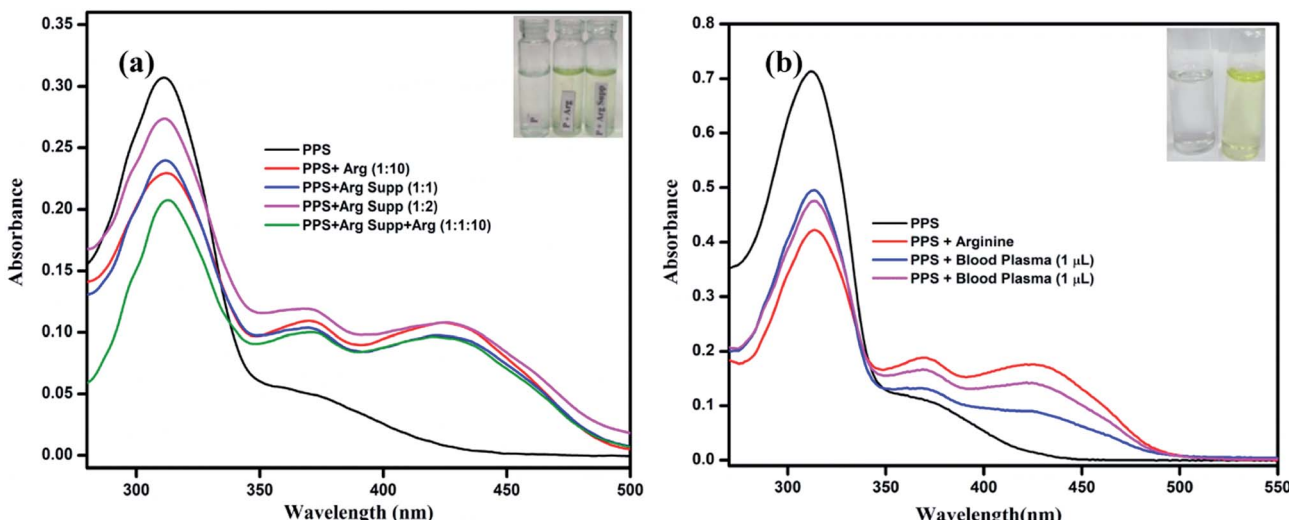


Fig. 10 (a) Colorimetric detection of arginine by PPS in arginine supplements. (b) Colorimetric detection of arginine by PPS in human blood plasma.

towards arginine, L-arginine granules were selected as a real sample. 250 mg of these granules were dissolved in 5 mL of distilled water and the solution was filtered. Two samples were prepared by adding 10  $\mu$ L and 20  $\mu$ L of this solution to a 3 mL solution of **PPS** (10  $\mu$ M, DMSO-PBS, pH = 7.4, 8 : 2, v/v). Another sample was prepared by spiking 100  $\mu$ M of arginine solution into a solution of **PPS** containing 10  $\mu$ L of granule solution. The absorption spectra of these samples were recorded, as can be seen in Fig. 10(a). The absorption spectrum of **PPS** containing arginine granules showed a similar pattern to that of **PPS**-arginine. Therefore it can be inferred that **PPS** has the potential to be used in real sample analysis.

**3.11.2 Detection of arginine in blood plasma.** To further examine the utility of **PPS** in humans, we were inspired to detect arginine in biological samples as well. In blood, low molecular weight arginine is present in the free state and is also bound to proteins in which it is present in higher percentages. For the present study to determine arginine in biological samples, we used blood plasma as a source. The additions of human blood plasma to **PPS** lead to a color change in the probe along with changes in the UV-vis absorption spectra. The color change of the solution from colorless to yellow was readily detectable by the naked eye. Also, the absorption spectra showed a decrease in the band intensity at 320 nm and the formation of a new band at 410 nm (Fig. 10(b)). These observations were the same as those in the experiments performed above. Therefore, it is worth mentioning that **PPS** is a potential chemosensor for the selective detection of arginine over other amino acids in human blood plasma.

## 4. Conclusions

In conclusion, a novel Schiff base **PPS** has been successfully synthesized by the condensation reaction of aldehyde and hydrazine derivatives of pyranopyrazole. The formation of **PPS** was confirmed through NMR, IR and mass spectrometry. **PPS**

acted as a turn-on colorimetric sensor for the amino acid arginine in DMSO-PBS (8 : 2 v/v, 10 mM, pH = 7.4). Arginine formed a 1 : 1 complex with **PPS** with binding constant  $K_a = 8.57 \times 10^4 \text{ M}^{-1}$ , as evident from the Job's plot and Benesi-Hildebrand plot, respectively. Selectivity studies revealed that **PPS** acted as a selective chemosensor for arginine in the presence of other amino acids; however, interference was observed in the presence of Cys and GSH. The detection limit of **PPS** for arginine was found to be  $1.8 \times 10^{-5} \text{ M}$ . The formation of a **PPS**-arginine complex was established using  $^1\text{H}$  NMR titration and DFT experiments. **PPS**-arginine formed *in situ* was found to show reversible absorption and colorimetric response towards  $\text{H}_2\text{PO}_4^-$ . Moreover, **PPS** could efficiently detect arginine in arginine supplement granules and blood plasma. Therefore, it could be inferred that the chemosensor **PPS** acted as a potential sensor for arginine in real samples.

## Conflicts of interest

The authors declare no conflict of interest.

## Acknowledgements

R. B thanks the Council of Scientific & Industrial Research (CSIR) for providing fellowship. N. D and S. W would like to thank the University Grants Commission (UGC) for providing fellowship. R. K acknowledges the Institute of Eminence (IoE), University of Delhi for providing the grant to carry out the research work. The authors are also thankful to University Science Instrumentation Centre (USIC) for providing instrument facilities for carrying out this research work.

## References

- 1 J. Cao, L. Ding, W. Hu, X. Chen, X. Chen and Y. Fang, *Langmuir*, 2014, **30**, 15364–15372.



2 H. Tapiero, G. Mathé, P. Couvreur and K. Tew, *Biomed. Pharmacother.*, 2002, **56**, 439–445.

3 M. B. Witte and A. Barbul, *Wound Repair Regen.*, 2003, **11**, 419–423.

4 J. K. Stechmiller, B. Childress and L. Cowan, *Nutr. Clin. Pract.*, 2005, **20**, 52–61.

5 Y. Fang, T. Shane, F. Wu, C. Williams and C. Miller, *Biophys. J.*, 2010, **98**, 418a.

6 N. Guelzim, F. Mariotti, P. G. P. Martin, F. Lasserre, T. Pineau and D. Hermier, *Amino Acids*, 2010, **41**, 969–979.

7 G. Wu, F. W. Bazer, T. A. Davis, S. W. Kim, P. Li, J. M. Rhoads, M. C. Satterfield, S. B. Smith, T. E. Spencer and Y. Yin, *Amino Acids*, 2008, **37**, 153–168.

8 K. P. Nandre, S. V. Bhosale, K. V. S. R. Krishna, A. Gupta and S. V. Bhosale, *Chem. Commun.*, 2013, **49**, 5444–5446.

9 V. Gopalakrishnan, P. J. Burton and T. F. Blaschke, *Anal. Chem.*, 1996, **68**, 3520–3523.

10 K. A. Rawat and S. K. Kailasa, *Microchim. Acta*, 2014, **181**, 1917–1929.

11 D. L. Olson, M. E. Lacey, A. G. Webb and J. V. Sweedler, *Prog. Nucl. Magn. Reson. Spectrosc.*, 1995, **703**, 3070.

12 J. Williams, D. Lang, J. A. Smith and M. J. Lewis, *Biochem. Pharmacol.*, 1993, **46**, 2097–2099.

13 H. Chen, L. Gu, Y. Yin, K. Koh and J. Lee, *Int. J. Mol. Sci.*, 2011, **12**, 2315–2324.

14 K. Vishwanathan, R. L. Tackett, J. T. Stewart and M. G. Bartlett, *J. Chromatogr. B: Biomed. Sci. Appl.*, 2000, **748**, 157–166.

15 A. Mohammadi, B. Khalili and A. S. Haghayegh, *Spectrochim. Acta, Part A*, 2019, **222**, 117193.

16 R. Kumar, H. Jain, P. Gahlyan, A. Joshi and C. N. Ramachandran, *New J. Chem.*, 2018, **42**, 8567–8576.

17 K. Velugula and J. P. Chinta, *Biosens. Bioelectron.*, 2017, **87**, 271–277.

18 F. M. Abdelrazek, P. Metz, O. Kataeva, A. Jäger and S. F. El-Mahrouky, *Arch. Pharm.*, 2007, **340**, 543–548.

19 N. N. R. Y. Mohamed, A. F. Khaireldin, A. A. E. Fahmy, N. R. Mohamed, A. F. Fahmy, A. A. El-Sayed, D. Pharma, N. Y. Khaireldin, A. F. Fahmy and A. A. El-Sayed, *researchgate.net*, 2010, **2**, 400–417.

20 S. El-Assiery, G. Sayed and A. Fouada, *Acta Pharm.*, 2004, **54**, 143–150.

21 S. C. Kuo, L. J. Huang and H. Nakamura, *J. Med. Chem.*, 1984, **27**, 539–544.

22 T. UEDA, H. MASE, N. ODA and I. ITO, *Chem. Pharm. Bull.*, 1981, **29**, 3522–3528.

23 S. Wang, H. Ding, Y. Wang, C. Fan, G. Liu and S. Pu, *RSC Adv.*, 2019, **9**, 6643–6649.

24 J. Jiang, C. Gou, J. Luo, C. Yi and X. Liu, *Inorg. Chem. Commun.*, 2012, **15**, 12–15.

25 F. Wang, C. Feng, L. Lu, Z. Xu and W. Zhang, *Talanta*, 2017, **169**, 149–155.

26 M. Liu, Q. Jiang, Z. Lu, Y. Huang, Y. Tan and Q. Jiang, *Luminescence*, 2015, **30**, 1395–1402.

27 H. Jain, N. Deswal, A. Joshi, C. N. Ramachandran and R. Kumar, *Anal. Methods*, 2019, **11**, 3230–3243.

28 P. Gahlyan, R. Bawa, H. Jain, M. Dalela, A. Joshi, C. N. Ramachandran, A. K. Prasad, A. Kaur and R. Kumar, *ChemistrySelect*, 2019, **4**, 7532–7540.

29 R. Kumar, R. Bawa, P. Gahlyan, M. Dalela, K. Jindal, P. K. Jha, M. Tomar and V. Gupta, *Dyes Pigm.*, 2019, **161**, 162–171.

30 P. C. Hariharan and J. A. Pople, *Theor. Chim. Acta*, 1973, **28**, 213–222.

31 R. E. Skyner, J. L. McDonagh, C. R. Groom, T. van Mourik and J. B. O. Mitchell, *Phys. Chem. Chem. Phys.*, 2015, **17**, 6174–6191.

32 M. Dalela, T. G. Shrivastav, S. Kharbanda and H. Singh, *ACS Appl. Mater. Interfaces*, 2015, **7**, 26530–26548.

33 R. Kumar, N. Yadav, R. Lavilla, D. Blasi, J. Quintana, J. M. Brea, M. I. Loza, J. Mestres, M. Bhandari, R. Arora, R. Kakkar and A. K. Prasad, *Mol. Diversity*, 2017, **21**, 533–546.

34 A. Dreuw, J. L. Weisman and M. Head-Gordon, *J. Chem. Phys.*, 2003, **119**, 2943.

35 A. Dreuw and M. Head-Gordon, *J. Am. Chem. Soc.*, 2004, **126**, 4007–4016.

36 H. Yaku, T. Fujimoto, T. Murashima, D. Miyoshi and N. Sugimoto, *Chem. Commun.*, 2012, **48**, 6203–6216.

